Available online at www.sciencedirect.com
ScienceDirect
Trans. Nonferrous Met. Soc. China 35(2025) 3468−3479
Transactions of Nonferrous Metals Society of China
www.tnmsc.cn

Ion coordination affinity and its application in mineral flotation

Hong-liang ZHANG[1,2#], Xin RAO[1,2#], Chen-yang ZHANG[1,2], Jian-hua CHEN[3], Yang-ge ZHU[4], Rong WANG[1,2], Wei SUN[1,2]

1. School of Minerals Processing and Bioengineering, Central South University, Changsha 410083, China;
2. Engineering Research Center of Ministry of Education for Carbon Emission Reduction in Metal Resource Exploitation and Utilization, Central South University, Changsha 410083, China;
3. School of Resources, Environment and Materials, Guangxi University, Nanning 530000, China;
4. State Key Laboratory of Mineral Processing Science and Technology, Beijing General Research Institute of Mining & Metallurgy, Beijing 102628, China

Received 4 March 2024; accepted 18 September 2024

Abstract: The ion coordination affinities of the commonly found metal ions were evaluated using DFT calculations. The results indicate that the lowest unoccupied molecular orbital (LUMO) energy of metal ions correlates positively with their binding energies with O(S) ligands, and some metal ions with various valence states also present different affinities. Besides, due to the steric hindrance effects, the mono- and hexa-coordinated metal ions may exhibit different affinities, and the majority of the studied hexa-coordinated metal ions exhibit oxophilicity. These affinity differences perfectly illustrate the activation flotation practice in which the oxyphilic ions are applied to activating oxide minerals, while thiophilic ions are applied to activating sulfide minerals.

Key words: ion coordination affinity; mineral flotation; coordination chemistry; density functional theory

1 Introduction

Geochemical element affinity is a geological concept that describes the tendency of cations to selectively combine with specific anions in natural systems. GOLDSCHMIDT [1,2], through the analysis of extensive experimental data, classifies the geochemical affinity of elements into five categories: oxyphilic elements (lithophilic elements), thiophilic elements (cuprophilic elements), siderophile element, gas affine elements and biological affine elements. This classification is based on elements, but in nature, various elements exist in different valence states, which imposes limitations on its application.

The periodic table of elements and their ions, proposed by RAILBACK [3] in 2003 and grounded in the hard and soft acids and bases (HSAB) theory [4,5], categorizes elemental ions into six categories based on their valence state difference: noble gases (noble gases with no ionization), hard cations (cations with all electrons removed from outer shell), intermediate cations (cations with some electrons remaining in the outer shell), soft cations (cations with many electrons remaining in the outer shell), element forms (elemental forms with zero valence) and anions (anions that commonly coordinate with H^+). Furthermore, this table also illustrates the affinity of certain anions and cations for binding with one another. For instance, the order of binding capacity of common anions to hard

# Hong-liang ZHANG and Xin RAO contributed equally to this work
Corresponding author: Chen-yang ZHANG, Tel: +86-15573156566, E-mail: zhangchenyang@csu.edu.cn; Wei SUN, Tel: +86-13507310692, E-mail: sunmenghu@csu.edu.cn
https://doi.org/10.1016/S1003-6326(25)66893-2

cations is F > O > N = Cl > Br > I > S, while the order for soft cations is I > Br > S > Cl = N > O > F. Additionally, RAILBACK also noted the cations capable of forming simple sulfide and oxide minerals in the table, which serves as a significant reference.

Mineral processing is a discipline focused on the recovery of valuable elements, aiming to separate valuable minerals from gangue. Essentially, it is inseparable from the properties of various elemental ions. In froth flotation, the separation and purification of minerals strongly depend on the affinity or sparsity relationship between the flotation reagents and minerals [6], in which the reagents act directionally on the target mineral surface to achieve separation from other minerals. Consequently, understanding the affinities of various elemental ions is crucial for effective mineral flotation. Minerals in nature are primarily categorized into oxide minerals and sulfide minerals, with the elements present in these minerals exhibiting distinct affinity properties. For instance, Si is mainly found in silicate minerals, while Ca, Mg, Al, and Ba are primarily present in oxide minerals or oxygen-containing salt minerals in nature. Conversely, Mo is predominantly found in sulfide minerals such as molybdenite (MoS_2) [7].

The oxyphilic and thiophilic nature of elemental ions significantly influences the flotation separation of minerals. Normally, the oxyphilic oxide minerals are recovered by oxygen-terminated collectors, and the thiophilic sulfide minerals by sulfur-terminated collectors [8]. However, for strongly hydrophilic minerals, exogenous activator metal ions are often necessary [9]. For instance, quartz is collected by oleate (OL^-) with the help of Ca^{2+} ions [10], and sphalerite is collected by xanthate with the assistance of Cu^{2+} ions [11,12]. The mineral paragenesis is also related to ion affinity. For example, galena is frequently found in association with sphalerite in sulfide deposits [13]. Investigating ion affinity can yield new insights into mineral separation and smelting purification processes. A typical example is the separation of W and Mo based on their different thiophilicity. By introducing S^{2-} or HS^- as sulfidation reagents into the W solution, MoO_4^{2-} can be transformed into $MoO_xS_{(4-x)}^{2-}$ or even MoS_4^{2-}. The subsequent addition of Fe^{2+}, Cu^{2+} or Co^{2+} leads to the formation of precipitates with the thiomolybdates, which can then be removed [14].

Although element affinity is widely used in flotation practice, the systematic study of ion coordination affinity is still poorly reported. The previous research system mainly focused on simple M—S and M—O diatomics [15,16]. Flotation processes are complex and cannot be simplified to simple diatomic systems due to the various factors involved, such as solution environments, reagent types, mineral properties, and solid−liquid interface reactions. Thus, it is essential to consider the state of metal ions in minerals, solution environment, and solid−liquid interface to accurately determine their affinity in mineral flotation. In recent years, there have been reports of research on the coordination chemistry characteristics of reagents on minerals in academic literature [17]. Based on this fact, the investigation of the metal ion coordination affinity in the flotation process holds significant value in mineral processing. Thus, this study focuses on M—O(S)H_2 and M—6[O(S)H_2] cluster systems, representing monocoordinated and hexa-coordinated forms of metal ions, respectively. The selection of this system is based on the prevalence of hexa-coordinated structures among metal ions, either within mineral crystals or in solution environments.

The purpose of this work is to study the microscopic nature and general law of the ion coordination affinity through the first-principles calculation method and discuss its application in mineral flotation, so as to offer new lights for mineral separation and reagent development.

2 Computational details

2.1 Cluster model

Cluster models were performed with the Gaussian 16 quantum chemistry package, based on the WB97XD method [18]. The def2-TZVP (3-zeta basis set) [19], an all-electron basis set, was used in calculation for various cluster systems. The default convergence parameters in the Gaussian 16 software were retained to optimize the structure. All calculations were successfully converged, without virtual frequencies in the vibration analysis. The Mayer bond order was obtained by using Multiwfm program [20]. The binding energy (ΔG) between ligands and central metal ion can be calculated as follows [8]:

$$\Delta G=\frac{G_{\mathrm{M}-n\cdot\mathrm{Ligand}}-(G_{\mathrm{M}}+n\cdot G_{\mathrm{Ligand}})}{n} \quad (1)$$

where $G_{\mathrm{M}-n\cdot\mathrm{Ligand}}$ is the Gibbs free energy of the central metal ion with ligand coordinated, and G_{M}, and G_{Ligand} are the Gibbs free energies of central metal ion and ligand, respectively.

2.2 Periodic model

The DFT periodic models were conducted using the CASTEP program in Materials Studio 2020 [21]. The exchange−correlation potential was approximated within the GGA [22] using the PBESOL functional [23]. The correction for dispersion interaction was realized using the Grimme method [24]. The valence electron configurations for various atoms in this DFT calculation were S $3s^23p^4$, Cu $3d^{10}4s^1$, C $2s^22p^2$, O $2s^22p^4$, Na $3s^13p^0$ and H $1s^1$. The cutoff energy for the unit cell and slab model was set to be 500 and 400 eV with *k*-point sampling density of 6×6×6 and 1×1×1, respectively. In the calculations, charge compensation is performed for the charged system using counterions. The Dmol^3 program [25] is used for the calculation of frontier molecular orbital.

In this work, the quartz unit cell with the $P3\_121$ spatial group and sphalerite unit cell with $F\bar{4}3M$ spatial group were cited from Ref. [26] and Ref. [27] respectively. Quartz (101) [28] and sphalerite (110) [29] surfaces were selected as the test surfaces. The adsorption energy (E_{ads}) of adsorbate on mineral surface is given in the following definition:

$$E_{\mathrm{ads}}=E_{\mathrm{tot}}-E_{\mathrm{surface}}-E_{\mathrm{adsorbate}} \quad (2)$$

where E_{tot} is the total energy of the adsorption system, and E_{surface} and $E_{\mathrm{adsorbate}}$ refer to the energies of the mineral surface and adsorbate, respectively.

3 Results and discussion

3.1 Energy evaluation

Energy is an important indicator for evaluating the ion coordination affinity. Table 1 lists the binding energies of M—O(S)H_2 clusters. Generally speaking, hard cations are more oxyphilic, while soft cations are more thiophilic, with intermediate cations exhibiting comparable tendencies towards both oxygen and sulfur. Based on the data presented in Table 1, it can be observed that a significant proportion of intermediate cations and soft cations demonstrates a higher affinity towards H_2S in comparison to H_2O, as indicated by their more negative binding energies. The reason behind these results lies in the fact that the coordination atom S exhibits a lower electronegativity compared to O atom. Consequently, the disparity in electronegativity between the coordination atom S and the metal ions is smaller, resulting in a lower binding energy.

Table 1 Binding energies of different elements with single H_2O and H_2S

Cation	Classification	Binding energy/(kJ·mol^{-1})	
		M—OH_2	M—SH_2
Ti^{4+}	Inter	−1659.9	−
Mo^{4+}	Inter	−1379.8	−1816.2
W^{4+}	Inter	−1359.3	−1645.2
Co^{3+}	Inter	−1078.0	−
Mn^{3+}	Inter	−1015.7	−1258.2
Fe^{3+}	Inter	−972.7	−1442.1
Cr^{3+}	Inter	−789.2	−1109.8
Al^{3+}	Inter	−786.3	−940.9
Sc^{3+}	Inter	−615.7	−654.6
Sb^{3+}	Soft	−606.9	−687.2
Ni^{2+}	Inter	−462.3	−619.1
Zn^{2+}	Inter	−389.6	−463.1
Mn^{2+}	Inter	−367.8	−331.9
Cu^{2+}	Soft	−362.4	−553.9
Co^{2+}	Inter	−338.2	−403.8
Cd^{2+}	Soft	−304.3	−376.2
Mg^{2+}	Hard	−297.6	−273.0
Sn^{2+}	Soft	−256.4	−224.3
Fe^{2+}	Inter	−236.2	−285.1
Pb^{2+}	Soft	−222.4	−215.7
Ca^{2+}	Hard	−209.4	−137.1
Ba^{2+}	Hard	−151.3	−97.8
Ag^{+}	Soft	−103.2	−137.1

The classification type of hard (hard cations), inter (intermediate cations) and soft (soft cations) were defined by RAILSBACK in 2003 [3]

W^{4+} and Mo^{4+}, classified as intermediate cations in Group VIB of the periodic table, are

chemically very similar and both show strong thiophilicity, with Mo^{4+} being stronger than W^{4+}. However, there is no significant difference in their oxophilicity. Mn^{2+}, Mg^{2+}, Sn^{2+}, Ca^{2+} and Ba^{2+} are more suitable to bond with O ligand than S ligand according to the binding energy, showing the oxophilicity. The cations, Mg^{2+}, Ba^{2+} and Ca^{2+}, which are classified as hard cations situated in Group IIA, exhibit binding energies to the ligand oxygen that align with the trend of ionic potential as defined by RAILSBACK [3], specifically Mg^{2+}> Ca^{2+}>Ba^{2+}. For Pb^{2+}, classified as a soft cation, appears to have thiophilicity that is comparable to its oxophilicity, albeit with a slight preference for oxophilicity. This characteristic may account for the ease with which surface-exposed galena is transformed into a series of secondary oxide minerals, such as anglesite and cerussite.

Al^{3+}, classified as a hard cation, demonstrates thiophilicity according to binding energy results. However, in reality, aluminum exhibits a strong affinity for oxygen [30]. Aluminum sulfide is almost non-existent in nature, which can be attributed to its instability and tendency to hydrolyze upon contact with water, resulting in the formation of $Al(OH)_3$ and the water-insoluble H_2S [31]. In addition, ion coordination affinity is significantly influenced by the valence state of ions. Generally, cations with a higher valence state demonstrate a stronger binding ability to ligands. Moreover, ions of the same element but with different valence states can exhibit varying affinities. For example, Mn^{3+} shows a preference for binding with S ligands, while Mn^{2+} displays a greater affinity for O ligands.

3.2 Bond order information

The chemical bond nature is crucial in determining ion coordination affinities. Table 2 presents the Mayer bond orders of M—O(S) in M — $O(S)H_2$ clusters. The Mayer bond order essentially reflects the number of electron pairs shared between two atoms [32]. According to Table 2, it is evident that the Mayer bond order of the bond formed between the metal ion and the S ligand is greater than that with the O ligand. This indicates that the metal ion shares more electron pairs with the S ligand, resulting in a stronger covalent character of the M — S bond. In coordination compounds, the strength of covalent bonds can reflect the stability of coordination compounds to some extent. This result aligns with the Nephelauxetic effect [33], which characterizes covalency; specifically, the smaller the electro-negativity of the corresponding ligand, the greater the Nephelauxetic effect of the metal ions and the stronger the covalence of the coordination bond.

Table 2 Mayer bond order of center metal ions and ligand O and S atoms in M—$O(S)H_2$ clusters

Cluster	M—O	M—S
Ti^{4+}	1.2	−
Mo^{4+}	1.48	1.57
W^{4+}	1.55	1.81
Co^{3+}	1.47	−
Mn^{3+}	1.3	1.67
Fe^{3+}	1.25	1.45
Cr^{3+}	0.73	1.62
Al^{3+}	1.22	1.17
Sc^{3+}	0.89	1.18
Sb^{3+}	0.92	1.41
Ni^{2+}	0.98	1.13
Zn^{2+}	0.7	1.03
Mn^{2+}	0.68	1.14
Cu^{2+}	0.66	0.67
Co^{2+}	0.81	1.48
Cd^{2+}	0.5	0.94
Mg^{2+}	0.3	0.76
Sn^{2+}	0.49	0.84
Fe^{2+}	0.73	1.48
Pb^{2+}	0.41	0.77
Ca^{2+}	0.24	0.4
Ba^{2+}	0.11	0.3
Ag^{+}	0.28	0.69

3.3 Hexa-coordinated M—6[$O(S)H_2$] cluster

The results of mono-coordination indicate that ion coordination affinity is universal and adheres to specific rules. Given that the metal ions are constrained by the crystal field, the hexa-coordinated M — 6[$O(S)H_2$] clusters of metal cations are subsequently constructed based on the findings from the mono-coordinated clusters. The

average binding energies, which are utilized to assess ion coordination affinity, are presented in Table 3.

Table 3 Average binding energies of elements with six H_2O and H_2S (kJ/mol)

Cation	M—6(OH_2)	M—6(SH_2)
Mo^{6+}	−1613.9	−1748.7
W^{6+}	−1505.0	−1713.6
Mn^{4+}	−897.6	−
Ti^{4+}	−720.2	−703.5
Mo^{4+}	−678.8	−696.0
Sn^{4+}	−673.8	−694.7
W^{4+}	−673.0	−675.5
Zr^{4+}	−557.6	−523.3
Co^{3+}	−519.6	−521.2
Fe^{3+}	−491.2	−483.6
Mn^{3+}	−462.3	−443.5
$Al^{3+;}$	−439.7	−386.7
Cr^{3+}	−437.6	−410.9
Sc^{3+}	−345.3	−296.4
Sb^{3+}	−312.1	−303.9
Fe^{2+}	−228.2	−202.3
Cu^{2+}	−213.2	−189.8
Zn^{2+}	−204.0	−173.1
Mg^{2+}	−205.9	−128.7
Ca^{2+}	−135.0	−90.3
Sn^{2+}	−130.8	−102.4
Pb^{2+}	−122.5	−98.2
Ba^{2+}	−104.1	−60.6

Mo and W, as transition metal elements, are traditionally categorized as oxyphilic and thiophilic elements, respectively. This classification is supported by the average binding energies of W^{4+} and Mo^{4+} with S ligands, which confirms that Mo exhibits greater thiophilicity than W. Furthermore, SUN and ZHAO [34] believed that Mo, both tetravalent and hexavalent, has a stronger thiophilicity than W.

The tetravalent Ti ion is classified as a hard cation with strong oxophilicity, consistent with its natural occurrence in the form of TiO_2. Within the category of trivalent ions, elements such as Fe, Mn, Al, Cr, and Sc exhibit oxyphilic properties, demonstrating a greater affinity for O ligands compared to S ligands, as evidenced by their more negative average binding energies. As shown in Table 1, Sc displays different affinities in mono- and hexa-coordinated clusters, with mono-coordination being thiophilic and hexa-coordination being oxyphilic. Sb is categorized as a thiophilic element, whereas Sb^{3+} is classified as a hard cation. According to the HSAB theory, Sb^{3+} is considered a boundary acid, with no apparent bonding affinity to sulfur or oxygen ligands. This supports the finding that the average binding energies of the hexa-coordinated M—6[$O(S)H_2$] clusters are closely aligned. Furthermore, this explains that in nature, Sb is not only found in the sulfide mineral form of stibnite (Sb_2S_3) but also in the oxide form of valentinite (Sb_2O_3). The divalent ions, Mg^{2+}, Ca^{2+}, and Ba^{2+}, are recognized as hard cations, exhibiting oxophilicity. In contrast, the divalent ions, Fe^{2+}, Cu^{2+}, Sn^{2+}, Pb^{2+}, and Zn^{2+}, are categorized as boundary acids, displaying similar binding strengths to the ligands S and O in the hexa-coordinated M—6[$O(S)H_2$] clusters that are similar.

3.4 Ligand field effect

Figure 1 shows the hexa-coordinated clusters of several common metal ions. From the perspective of coordination chemistry, transition metal ions exhibit different electron configurations following the splitting of d orbitals, which is influenced by the type of ligands involved, as determined by the splitting energy and electron pairing energy. For Cu^{2+} with d^9 electronic configuration, the electron arrangement after d orbital splitting is $(t_{2g})^6(e_g)^3$. This arrangement leads to an uneven distribution of electrons between the d_{z^2} and $d_{x^2-y^2}$ orbitals, resulting in the Jahn−Teller effect and the formation of a stretched octahedron configuration. A similar phenomenon can also be observed in transition metal ions with d^4 electronic configurations. When Cu^{2+} forms hexa-coordinated clusters with H_2O and H_2S, as shown in Fig. 1, a pronounced Jahn−Taylor effect occurs, leading to the elongation of the axial bonds. A pertinent example is the Cu atom in malachite [35].

Metal ions typically form hexa-coordinated structures with O ligands and four-coordinated structures with S ligands, depending on the radius

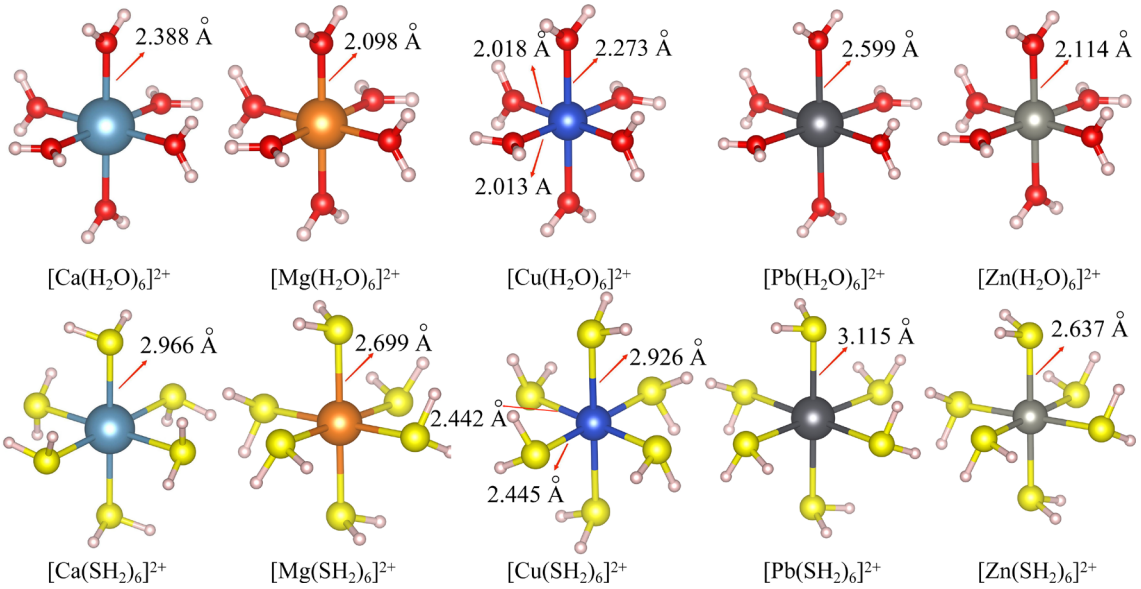

Fig. 1 Hexa-coordinated clusters of some common metal ions

of the central atom. Larger-radius S ligands appear to be less able to accumulate in large numbers around small-radius metal ions due to spatial hindrance effects. As illustrated in Fig. 2, derived from the data in Fig. 1 (the average bond length in the *XY* plane), the average distances between Cu—O and Cu—S in the *XY* plane are observed to be 2.02 and 2.44 Å, respectively. The calculated distance between adjacent O atoms in Fig. 2(a) is 2.86 Å, which is slightly larger than the sum of the radii of two O atoms (2.8 Å). This finding indicates that there is no spatial hindrance between adjacent O atoms in the Cu—O interaction within the *XY* plane, suggesting that Cu can form a six-coordinate structure with O ligands without spatial hindrance. In contrast, the calculated distance between adjacent S atoms in Fig. 2(b) is 3.45 Å, which is smaller than the sum of the radii of two S atoms (3.68 Å). This suggests that spatial hindrance exists between adjacent S atoms in the Cu—S interaction in *XY* plane, negatively impacting the formation of a hexa-coordinated structure with Cu and S ligands. Furthermore, the average binding energy of the hexa-coordinated clusters presented in Table 3 reinforces this conclusion. Thus, the tendency of most metal ions in this study to form hexa-coordinated clusters with H_2O can be attributed to the influence of steric hindrance.

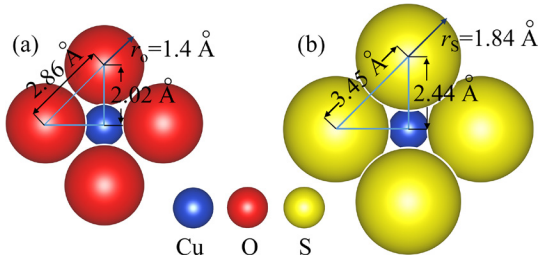

Fig. 2 Cu—O (a) and Cu—S (b) in *XY* plane during hexa-coordination

3.5 Orbital properties

Frontier molecular orbitals serve as frontline positions for the interaction between the central atom and the ligand atoms, and can be utilized to predict molecular reaction activity [36]. When H_2O and H_2S coordinate with cations, the central cation primarily provides an empty orbital, and the ligand contributes lone pair electrons, resulting in the formation of a coordinate covalent bond. This process predominantly involves the lowest unoccupied molecular orbital (LUMO) of the ions and the highest occupied molecular orbital (HOMO) of the ligands. In this study, the ligands are H_2O and H_2S, making the LUMO of the central ion a critical factor influencing reactivity. As illustrated in Fig. 3, the relationship between the average binding energies of the hexa-coordinated M—6[O(S)H_2] clusters and the LUMO energy of the central ion is depicted. The data indicate a strong correlation between the binding energies and the LUMO energy of the central cations, specifically, a lower LUMO energy corresponds to a more negative binding energy. This suggests that the LUMO of the central cation is a significant factor affecting the binding energy.

3.6 Application in quartz activation flotation

A typical flotation case based on ion coordination affinity is the activated flotation of quartz in oleate system. This is attributed to the strong hydroxylation behavior of the quartz surface, where the hydroxylated quartz surface forms a layer of oxygen-terminated structures that are oxyphobic but hydrophilic [37], which can prevent the interface reaction of the oxygen-terminated collectors (normally oleate). Given the strong hydroxylation behavior of the quartz surface, it is not possible to achieve flotation of quartz using oleate alone. In essence, the presence of interfacial hydration structure causes the collector OL^- losing action sites, and OL^- can only be adsorbed on the quartz surface via hydrogen bonding, as shown in Fig. 4(a). The hydrated surface structure presented in Fig. 4 is consistent with previous studies [38], with the difference that both the top and bottom surfaces of quartz are subjected to hydration treatment. In this adsorption mode, the two O atoms at the end of oleate form two hydrogen bonds with bond lengths of 1.59 and 1.74 Å on the hydroxylated quartz surface, yielding an adsorption energy of −61.2 kJ/mol, which suggests that OL^- cannot form an effective adsorption on the hydrated quartz surface from a thermodynamic perspective.

Therefore, a viable flotation scheme involves bridging the two oxygen-terminated substances, quartz and oleate. This requires the presence of an oxyphilic bridge, which is fundamental to the Ca^{2+} activation of quartz. In Fig. 4(b), the Ca^{2+} ion adsorbs onto the hydroxylated quartz surface, forming three Ca—O bonds, namely Ca—O_{m1} (2.37 Å), Ca—O_{h1} (2.38 Å), and Ca—O_{h2} (2.44 Å), with an adsorption energy of −197.1 kJ/mol. Additionally, the Mulliken bond populations for Ca—O_{m1}, Ca—O_{h1}, and Ca—O_{h2} bonds are −0.09, −0.03, and −0.02, respectively, indicating that the Ca—O bonds formed by the adsorption of Ca^{2+} are ionic bonds. The modification of the quartz surface by the oxyphilic Ca^{2+} ion creates an optimal

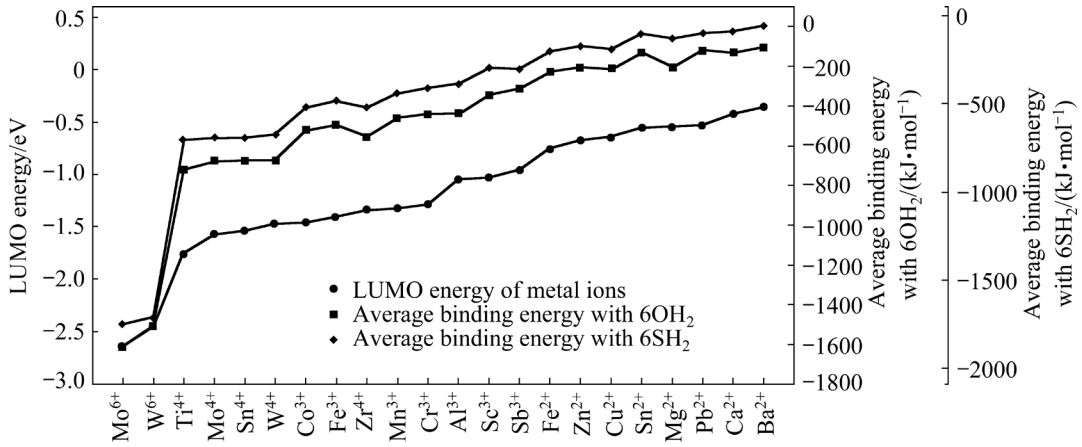

Fig. 3 Relationship between binding energy of metal ions with ligands in hexa-coordinated M—6[O(S)H_2] clusters, and LUMO energy of metal ions

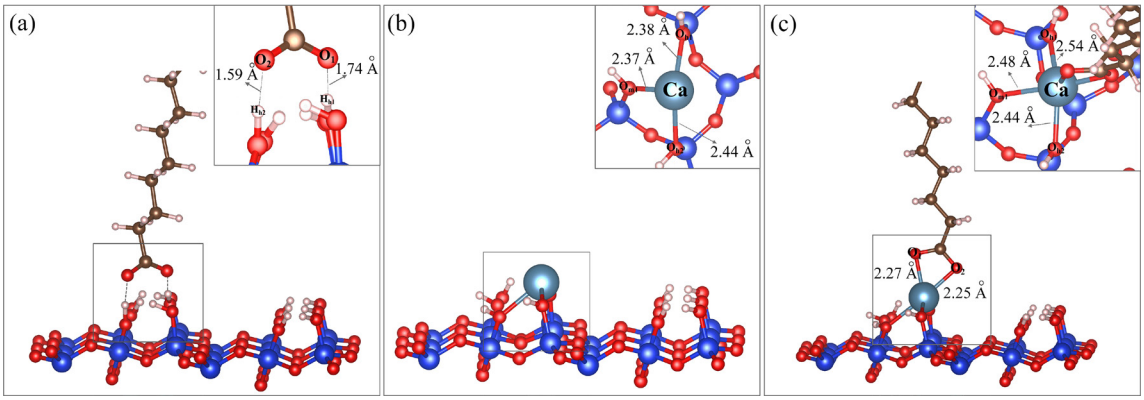

Fig. 4 Adsorption configuration of reagents: (a) OL^- on quartz (101) hydroxylated surface; (b) Ca^{2+} cation on quartz (101) hydroxylated surface; (c) OL^- adsorbed on Ca^{2+} activated quartz surface

adsorption site for the subsequent interfacial adsorption of OL^-, as illustrated in Fig. 4(c). At the adsorption interface, Ca^{2+} adopts a five-coordinated structure with adsorption energy of −521.2 kJ/mol, which significantly exceeds that of the direct adsorption (−61.2 kJ/mol) of OL^-. The Mulliken bond populations for Ca—O_1 and Ca—O_2 formed by the adsorption of OL^- at the surface Ca site are 0.10 and 0.11, respectively, indicating that these bonds are slightly stronger than the ionic bonds formed by the Ca ions on the quartz surface.

Table 4 presents the parameters of adsorption energy, Mulliken bond population, and bond type throughout the quartz flotation process. The direct adsorption of OL^- on the hydration surface of quartz is weak hydrogen-bonding adsorption process, whereas the bridging adsorption mode of OL^- on the quartz surface mediated by the oxyphilic activation Ca^{2+} ion is a strong chemisorption process. It can be seen that the oxyphilic Ca^{2+} ion serving as a bridge between the two oxygen-terminated substances (collector OL and hydroxylated quartz) is the key to realize quartz flotation.

3.7 Application in sphalerite activation flotation

Another typical example of flotation based on elemental ion affinity is the activated flotation of sphalerite in the xanthate (BX^-) system, which utilizes the thiophilicity of the activator Cu^{2+} ion. In flotation, it is difficult to achieve sphalerite flotation using xanthate alone, although the exposed Zn sites on the sphalerite surface can be adsorbed by the xanthate, forming two Zn—S bonds with bond length of 2.34 and 2.37 Å, respectively, as shown in Fig. 5(a). However, this mode of direct adsorption is relatively weak, with an adsorption energy of only −85.3 kJ/mol, making it difficult to achieve effective collection of sphalerite. It is interpreted that the $3d^{10}$ electronic configuration of Zn^{2+} on the sphalerite surface is very stable, rendering it difficult for Zn^{2+} ions to form π-back-donation bonds with collector BX^- [17]. In addition, it is also not in accordance with valence-bond theory as demonstrated in Fig. 5(b), where the symmetry of the HOMO of BX and that of the LUMO of sphalerite do not match each other. Although the energy gap between the two is very small, only 0.006 eV, similar results have also been reported by CHEN and LI [39]. Another contributing factor may be the steric hindrance effect associated with the direct adsorption of xanthate on the sphalerite surface [40]. Consequently, effective sphalerite flotation cannot be achieved without the introduction of activator metal ions.

Table 4 Changes of relevant parameters in process of Ca^{2+} activating quartz

Adsorption model	Adsorption energy/(kJ·mol^{-1})	Average Mulliken bond population of bonds generated by adsorption	Bonding form
OL^- on quartz (101) surface	−61.2	−	Hydrogen bond
Ca^{2+} on quartz (101) surface	−197.1	−0.05	Ionic bond
OL^- on Ca^{2+}-activated surface	−521.2	0.07	Ionic bond

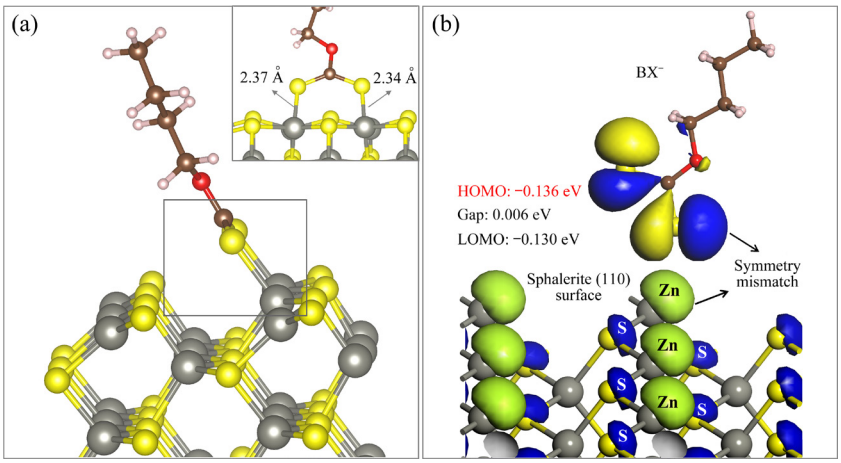

Fig. 5 Direct adsorption mode of BX^- on sphalerite surface: (a) Adsorption configuration; (b) Orbital symmetry

Figure 6(a) depicts adsorption configuration of Cu^{2+} on the sphalerite surface, which is consistent with the most stable adsorption configuration of Pb^{2+} on the surface of sphalerite, as reported by SARVARAMINI et al [41]. The Cu^{2+} ion forms bonds with three S atoms on the sphalerite surface, specifically Cu—S_{m1} (2.43 Å), Cu—S_{m2} (2.44 Å), and Cu — S_{m3} (2.40 Å), with corresponding Mulliken bond populations of 0.26, 0.26, and 0.09, respectively. Additionally, Cu^{2+} shares electrons with the adjacent Zn_1 atom. The adsorption energy of activator Cu^{2+} ion on the sphalerite surface is −210.7 kJ/mol. Figure 6(b) presents the adsorption configuration of BX^- on the Cu^{2+}-activated sphalerite surface, where Cu^{2+} significantly relaxes upward, ultimately aligning with the Zn and S atoms in the first surface layer. The position of Cu^{2+} resembles the stacking position of the Zn atom in the crystal structure. Cu^{2+} detaches from the S_{m3} atom and moves further away from the surface Zn_1 atom. Furthermore, the Cu^{2+} ion bonds with two S atoms of xanthate after breaking the Cu—S_{m1} bond, resulting in a planar triangular coordination structure. The adsorption energy of BX^- on the Cu^{2+}-activated sphalerite surface is −413.2 kJ/mol, which is stronger than the direct adsorption of BX^- on the surface Zn site. Therefore, the introduction of thiophilic Cu^{2+} ions is the preferred option to recover sphalerite with xanthate in flotation practices.

Figure 7 illustrates the electron density difference during the activation process of Cu^{2+}. It is evident that electrons accumulate between Cu and S atoms, suggesting that these atoms share electrons and form covalent bonds. Figures 7(a, b) demonstrate that the Cu^{2+} ion adsorbed on the sphalerite surface gains electrons, resulting in a decrease in the Hirshfeld charge. Subsequently, during the adsorption of BX^-, the Cu^{2+} ion loses some electrons, causing the Hirshfeld charge to

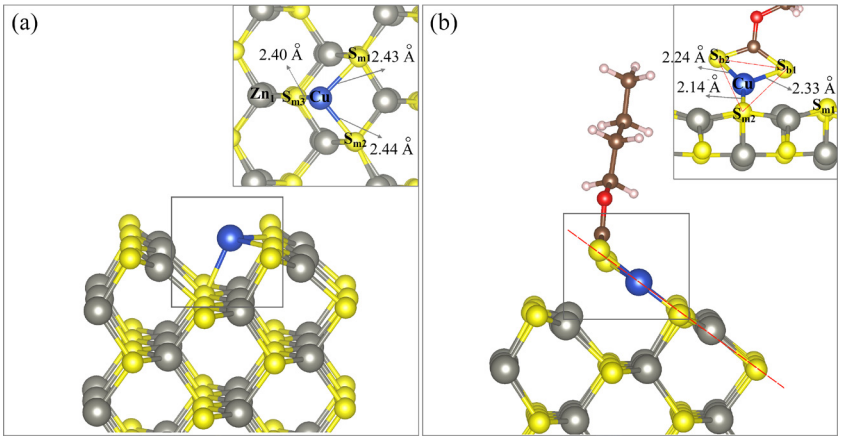

Fig. 6 Cu^{2+}-mediated bridging adsorption mode: (a) Cu^{2+} adsorbed on sphalerite surface; (b) BX^- adsorbed on Cu^{2+}-activated sphalerite surface

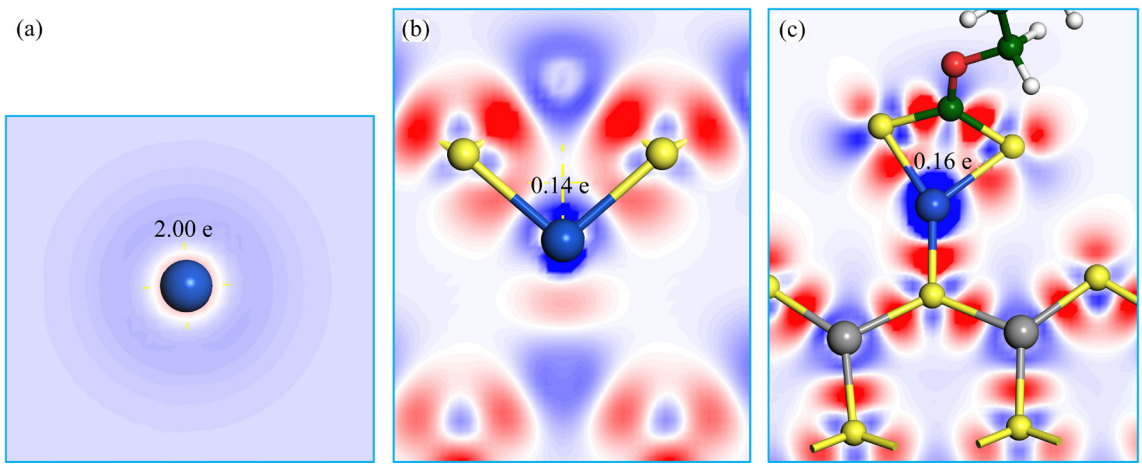

Fig. 7 Electron density difference: (a) Cu^{2+}; (b) Cu^{2+} adsorbed on sphalerite surface; (c) BX^- adsorbed on Cu^{2+}-activated sphalerite surface

increase from 0.14 to 0.16. This charge increase occurs because the Cu site loses electrons as it disconnects from the S_{m1} and S_{m2} atoms during the upward relaxation. Furthermore, the relaxed Cu site no longer shares electrons with the Zn_1 atom, which also significantly contributes to the elevated charge. Indeed, this is supported by the Hirshfeld charges of S_{b1} and S_{b2} in BX^-, which decrease from −0.15 and −0.17 to −0.07 and −0.10, respectively, after the adsorption of BX^- onto the surface Cu site, as given in Table 5. In summary, the Cu^{2+} ion serves as an effective activator for sphalerite flotation in the xanthate system, attributed to its stronger thiophilicity compared to the Zn^{2+} ion.

Table 5 Hirshfeld charge before and after adsorption of BX^- on Cu^{2+}-activated sphalerite surface (e)

Status	Cu	Zn_1	S_{m1}	S_{m2}	S_{m3}	S_{b1}	S_{b2}
Before BX^- adsorption	0.14	0.21	−0.25	−0.25	0.21	−0.15	−0.17
After BX^- adsorption	0.16	0.22	−0.26	−0.24	−0.22	−0.07	−0.10

4 Conclusions

(1) The ion coordination affinity is significantly influenced by the valence state of ions. The higher the valence state of cations, the stronger the binding ability to the ligands. Even, ions of the same element with different valence states may show different affinities.

(2) Since the S ligand with larger radius is difficult to accumulate in large numbers around small-radius metal ions due to spatial hindrance effects. The divalent ions, Cu^{2+} and Zn^{2+}, show thiophilicity in the mono-coordinated clusters, and oxophilicity in the hexa-coordinated clusters.

(3) The binding energy of the metal ion with the ligands of S and O is found to correlate positively with the LUMO energy of the metal ion, in that the lower the LUMO energy, the more negative the binding energy.

(4) Oxyphilic ions and thiophilic ions can be used for interfacial activation of refractory oxide minerals in oxygen-terminated collector systems and activation flotation of sulfide minerals under the sulfur-terminated collector system, respectively.

(5) In the subject (mineral processing) dominated by colloids and interfaces, ion affinity is expected to provide new lights on the development of mineral-specific flotation reagents, and to be a topical concern in the subject.

CRediT authorship contribution statement

Hong-liang ZHANG: Writing − Original draft, Conceptualization, Formal analysis, Software, Writing − Review & editing; **Xin RAO:** Writing − Original draft, Formal analysis, Software, Writing − Review & editing; **Chen-yang ZHANG:** Supervision, Methodology, Funding acquisition, Writing − Review & editing; **Jian-hua CHEN:** Formal analysis, Visualization, Writing − Review & editing; **Yang-ge ZHU:** Investigation, Data curation, Writing − Review & editing; **Rong WANG:** Visualization, Writing − Review & editing, Validation; **Wei SUN:** Supervision, Methodology, Funding acquisition, Writing − Review & editing.

Declaration of competing interest

The authors declare that they have no known competing financial interests or personal relationships that could have appeared to influence the work reported in this paper.

Acknowledgments

This work was financially supported by the National Natural Science Foundation of China (Nos. 52074356, U20A20269); the Key Technology Research and Development Program, China (No. 2022YFC2904503); the Special Fund for the Construction of Hunan Province, China (No. 2023SK2061); the Science and Technology Innovation Program of Hunan Province, China (No. 2022RC1183); the Changsha Science and Technology Project (Changsha Outstanding Innovative Youth Training Program), China; Innovation-driven Project of Central South University, China (No. 2023CXQD002); Higher Education Discipline Innovation Project, China (No. B14034). This work was carried out in part using hardware and/or software provided by the High-Performance Computing Centers of Central South University (China).

References

[1] GOLDSCHMIDT V M. The geochemical background of minor-element distribution [J]. Soil Science, 1945, 60: 1−8.

[2] GOLDSCHMIDT V M. The principles of distribution of chemical elements in minerals and rocks. [J]. Journal of the Chemical Society (Resumed), 1937: 655−673.

[3] RAILSBACK L B. An earth scientist's periodic table of the elements and their ions [J]. Geology, 2003, 31: 737−740.

[4] PEARSON R G. Hard and soft acids and bases, HSAB,

part 1: Fundamental principles [J]. Journal of Chemical Education, 1968, 45: 581−587.

[5] PEARSON R G. Hard and soft acids and bases, HSAB, part II: Underlying theories [J]. Journal of Chemical Education, 1968, 45: 643−648.

[6] LIU Sheng, LIU Guang-yi, HUANG Yao-guo, ZHONG Hong. Hydrophobic intensification flotation: Comparison of collector containing two minerophilic groups with conventional collectors [J]. Transactions of Nonferrous Metals Society of China, 2020, 30: 2536−2546.

[7] LI Zeng, WANG Man, XIAO Chao, WU Sheng-xi, ZHANG Gui-qing, GUAN Wen-juan, LI Qing-gang, CAO Zuo-ying. Enhancement of $CaMoO_4$ calcine decomposition and recovery of calcium resource by HCl cycle leaching [J]. Transactions of Nonferrous Metals Society of China, 2022, 32: 1314−1324.

[8] ZHANG Hong-liang, SUN Wei, ZHANG Chen-yang, HE Jian-yong, CHEN Dai-xiong, ZHU Yang-ge. Adsorption performance and mechanism of the commonly used collectors with oxygen-containing functional group on the ilmenite surface: A DFT study [J]. Journal of Molecular Liquids, 2022, 346: 117829.

[9] ZHANG Hong-liang, LIN Shang-yong, GUO Zhi-hao, SUN Wei, ZHANG Chen-yang. Selective separation mechanism of hematite from quartz by anionic reverse flotation: Implications from surface hydroxylation [J]. Applied Surface Science, 2023, 614: 156056.

[10] CAO Shao-hang, YIN Wan-zhong, YANG Bin, ZHU Zhang-lei, SUN Hao-ran, SHENG Qiu-yue, CHEN Ke-qiang. Insights into the influence of temperature on the adsorption behavior of sodium oleate and its response to flotation of quartz [J]. International Journal of Mining Science and Technology, 2022, 32: 399−409.

[11] WEI Qian, JIAO Fen, DONG Liu-yang, LIU Xue-duan, QIN Wen-qing. Selective depression of copper-activated sphalerite by polyaspartic acid during chalcopyrite flotation [J]. Transactions of Nonferrous Metals Society of China, 2021, 31: 1784−1795.

[12] QIU Ting-sheng, LI Guo-dong, LI Xiao-bo, YAN Hua-shan, LIU Chen. Influence of high concentration Zn^{2+} on floatability of sphalerite in acidic system [J]. Transactions of Nonferrous Metals Society of China, 2021, 31: 2128−2138.

[13] ZHANG Li-min, GAO Jian-de, KHOSO S. A, WANG Li, LIU Yu-ling, GE Peng, TIAN Meng-jie, SUN Wei. A reagent scheme for galena/sphalerite flotation separation: Insights from first-principles calculations [J]. Minerals Engineering, 2021, 167: 106885.

[14] ZHAO Zhong-wei, GAO Li-li, CAO Cai-fang, LI Jiang-tao, CHEN Xing-yu, CHEN Ai-liang, LIU Xu-heng, SUN Pei-mei, HUO Guang-sheng, LI Yun-jiao, LI Hong-gui. Separation of molybdenum from tungstate solution — Scavenging thiomolybdate by copper compound [J]. Metallurgical and Materials Transactions B, 2012, 43: 1284−1289.

[15] KEPP K P. A Quantitative scale of oxophilicity and thiophilicity [J]. Inorganic Chemistry, 2016, 55: 9461−9470.

[16] MOLTVED K A, KEPP K P. The chemical bond between transition metals and oxygen: Electronegativity, d-orbital effects, and oxophilicity as descriptors of metal–oxygen interactions [J]. The Journal of Physical Chemistry C, 2019, 123: 18432−18444.

[17] CHEN Jian-hua. Coordination principle of minerals flotation [M]. Singapore: Springer Nature Singapore, 2022.

[18] CHAI J D, HEAD-GORDON M. Long-range corrected hybrid density functionals with damped atom-atom dispersion corrections [J]. Phys Chem Chem Phys, 2008, 10: 6615−6620.

[19] WEIGEND F, AHLRICHS R. Balanced basis sets of split valence, triple zeta valence and quadruple zeta valence quality for H to Rn: Design and assessment of accuracy [J]. Phys Chem Chem Phys, 2005, 7: 3297−3305.

[20] LU Tian, CHEN Fei-wu. Multiwfn: A multifunctional wavefunction analyzer [J]. Journal of Computational Chemistry, 2012, 33: 580−592.

[21] PAYNE M C, TETER M P, ALLAN D C, ARIAS T A, JOANNOPOULOS J D. Iterative minimization techniques for ab initio total-energy calculations: Molecular dynamics and conjugate gradients [J]. Reviews of Modern Physics, 1992, 64: 1045−1097.

[22] PERDEW J P, CHEVARY J A, VOSKO S H, JACKSON K A, PEDERSON M R, SINGH D J, FIOLHAIS C. Atoms, molecules, solids, and surfaces: Applications of the generalized gradient approximation for exchange and correlation [J]. Physical Review B, 1992, 46: 6671−6687.

[23] HAMMER B, HANSEN L B, NØRSKOV J K. Improved adsorption energetics within density-functional theory using revised Perdew−Burke−Ernzerhof functionals [J]. Physical Review B, 1999, 59: 7413−7421.

[24] GRIMME S, ANTONY J, EHRLICH S, KRIEG H. A consistent and accurate ab initio parametrization of density functional dispersion correction (DFT-D) for the 94 elements H-Pu [J]. J Chem Phys, 2010, 132: 154104.

[25] DELLEY B. An all-electron numerical method for solving the local density functional for polyatomic molecules [J]. The Journal of Chemical Physics, 1990, 92: 508−517.

[26] GUALTIERI A. Accuracy of XRPD QPA using the combined Rietveld-RIR method [J]. Journal of Applied Crystallography, 2000, 33: 267−278.

[27] CHEN Jian-hua, CHEN Ye, LI Yu-qiong. Effect of vacancy defects on electronic properties and activation of sphalerite (110) surface by first-principles [J]. Transactions of Nonferrous Metals Society of China, 2010, 20: 502−506.

[28] MURASHOV V V, DEMCHUK E. A comparative study of unrelaxed surfaces on quartz and kaolinite, using the periodic density functional theory [J]. The Journal of Physical Chemistry B, 2005, 109: 10835−10841.

[29] WRIGHT K, WATSON G W, PARKER S C, VAUGHAN. D J. Simulation of the structure and stability of sphalerite (ZnS) surfaces [J]. American Mineralogist, 1998, 83: 141−146.

[30] MENG Jun-sheng, CHEN Ming-xuan, SHI Xiao-ping, MA Qiang. Effect of Co on oxidation and hot corrosion behavior of two nickel-based superalloys under Na_2SO_4−NaCl at 900 °C [J]. Transactions of Nonferrous Metals Society of China, 2021, 31: 2402−2414.

[31] LUO Xian-ping, ZOU Li-ping, MA Pei-long, LUO Cai-gui, XU Jing, TANG Xue-kun. Removing aluminum from a low-concentration lixivium of weathered crust elution-deposited rare earth ore with neutralizing hydrolysis [J]. Rare Metals,

2015, 36: 685−690.
[32] BRIDGEMAN A J, CAVIGLIASSO G, IRELAND L R, ROTHERY J. The Mayer bond order as a tool in inorganic chemistry [J]. Journal of the Chemical Society, Dalton Transactions, 2001, 14: 2095−2108.
[33] JØRGENSEN C K. In progress in inorganic chemistry [M]. United States: Wiley, 1962: 73−124.
[34] SUN Feng-long, ZHAO Zhong-wei. An interdisciplinary perspective from the earth scientist's periodic table: Similarity and connection between geochemistry and metallurgy [J]. Engineering, 2020, 6: 707−715.
[35] ZHANG Hong-liang, SUN Wei, QI-QI Zhou, XU Zhi-jie, CHEN Dai-xiong, ZHANG Chen-yang. Adsorption mechanism of water molecules on malachite surface [J]. The Chinese Journal of Nonferrous Metals, 2023, 33: 2318−2329. (in Chinese)
[36] FUKUI K. Role of frontier orbitals in chemical reactions [J]. Science, 1982, 218: 747−754.
[37] ZHANG Hong-liang, XU Zhi-jie, SUN Wei, ZHU Yang-ge, CHEN Dai-xiong, ZHANG Chen-yang. Hydroxylation structure of quartz surface and its molecular hydrophobicity [J]. Applied Surface Science, 2023, 612: 155884.
[38] ZHANG Hong-liang, XU Zhi-jie, SUN Wei, CHEN Dai-xiong, LI Sai, HAN Ming-jun, YU Heng, ZHANG Chen-yang. Selective adsorption mechanism of dodecylamine on the hydrated surface of hematite and quartz [J]. Separation and Purification Technology, 2021, 275: 119137.
[39] CHEN Jian-hua, LI Yu-qiong. Orbital symmetry matching study on the interactions of flotation reagents with mineral surfaces [J]. Minerals Engineering, 2022, 179: 8. 107469.
[40] CHEN Ye, LIU Xiao-mei, CHEN Jian-hua. Steric hindrance effect on adsorption of xanthate on sphalerite surface: A DFT study [J]. Minerals Engineering, 2021: 165: 106834.
[41] SARVARAMINI A, LARACHI F, HART B. Collector attachment to lead-activated sphalerite—Experiments and DFT study on pH and solvent effects [J]. Applied Surface Science, 2016, 367: 459−472.

离子配位亲和性及其在矿物浮选中的应用

张洪亮[1,2]，饶 鑫[1,2]，张晨阳[1,2]，陈建华[3]，朱阳戈[4]，王 嵘[1,2]，孙 伟[1,2]

1. 中南大学 资源加工与生物工程学院，长沙 410083；
2. 中南大学 金属资源开发利用碳减排教育部工程研究中心，长沙 410083；
3. 广西大学 资源环境与材料学院，南宁 530000；
4. 北京矿冶研究总院 矿物加工科学与技术国家重点实验室，北京 102628

摘 要：通过 DFT 计算评估常见金属离子的离子配位亲和性。结果表明，金属离子的最低空轨道(LUMO)能量与其与 O(S)配体的结合能呈正相关，一些不同价态的金属离子也表现出不同的亲和性。此外，由于空间位阻效应，单配位和六配位的金属离子可能表现出不同的亲和性，并且所研究大部分六配位金属离子表现出亲氧性。这些亲和性差异为深入理解矿物活化浮选的本质提供了重要视角，其中亲氧性离子用于活化氧化矿物，而亲硫性离子用于活化硫化矿物。

关键词：离子配位亲和性；矿物浮选；配位化学；密度泛函理论

(Edited by Bing YANG)